

## A SURVEY OF $Z \sim 6$ QUASARS IN THE SDSS DEEP STRIPE: I. A FLUX-LIMITED SAMPLE AT $Z_{AB} < 21$

LINHUA JIANG<sup>1</sup>, XIAOHUI FAN<sup>1</sup>, JAMES ANNIS<sup>2</sup>, ROBERT H. BECKER<sup>3,4</sup>, RICHARD L. WHITE<sup>5</sup>, KUENLEY CHIU<sup>6</sup>, HUAN LIN<sup>2</sup>, ROBERT H. LUPTON<sup>7</sup>, GORDON T. RICHARDS<sup>8</sup>, MICHAEL A. STRAUSS<sup>7</sup>, SEBASTIAN JESTER<sup>9</sup>, AND DONALD P. SCHNEIDER<sup>10</sup>

Submitted to AJ; August 19, 2007

### ABSTRACT

We present the discovery of five quasars at  $z \sim 6$  selected from 260 deg<sup>2</sup> of the Sloan Digital Sky Survey (SDSS) southern survey, a deep imaging survey obtained by repeatedly scanning a stripe along the Celestial Equator. The five quasars with  $20 < z_{AB} < 21$  are 1–2 magnitudes fainter than the luminous  $z \sim 6$  quasars discovered in the SDSS main survey. One of them was independently discovered by the UKIRT Infrared Deep Sky Survey. These quasars, combined with another  $z \sim 6$  quasar known in this region, make a complete flux-limited quasar sample at  $z_{AB} < 21$ . The sample spans the redshift range  $5.85 \leq z \leq 6.12$  and the luminosity range  $-26.5 \leq M_{1450} \leq -25.4$  ( $H_0 = 70$  km s<sup>-1</sup> Mpc<sup>-1</sup>,  $\Omega_m = 0.3$ , and  $\Omega_\Lambda = 0.7$ ). We use the  $1/V_a$  method to determine that the comoving quasar spatial density at  $\langle z \rangle = 6.0$  and  $\langle M_{1450} \rangle = -25.8$  is  $(5.0 \pm 2.1) \times 10^{-9}$  Mpc<sup>-3</sup> mag<sup>-1</sup>. We model the bright-end quasar luminosity function (QLF) at  $z \sim 6$  as a power law  $\Phi(L_{1450}) \propto L_{1450}^\beta$ . The slope  $\beta$  calculated from a combination of our sample and the luminous SDSS quasar sample is  $-3.1 \pm 0.4$ , significantly steeper than the slope of the QLF at  $z \sim 4$ . Based on the derived QLF, we find that the quasar/AGN population cannot provide enough photons to ionize the intergalactic medium (IGM) at  $z \sim 6$  unless the IGM is very homogeneous and the luminosity ( $L_{1450}^*$ ) at which the QLF power law breaks is very low.

*Subject headings:* galaxies: active — quasars: emission lines — quasars: general

### 1. INTRODUCTION

High-redshift quasars are among the most luminous objects known and provide direct probes of the distant universe when the first generation of galaxies and quasars formed. In recent years, over twenty  $z \sim 6$  quasars with  $z_{AB} \leq 20$  have been discovered (e.g. Fan et al. 2000, 2001a, 2003, 2004, 2006a; Goto 2006). These luminous quasars are essential for understanding the accretion history of black holes (BHs), galaxy formation, and chemical evolution at very early epochs. They harbor supermassive BHs with masses higher than  $10^9 M_\odot$  and emit near

the Eddington limit (e.g. Barth et al. 2003; Vestergaard 2004; Jiang et al. 2006a; Kurk et al. 2007), revealing the rapid growth of central BHs at high redshift. Their emission lines show solar or supersolar metallicity in the broad line regions, indicating that there was vigorous star formation and element enrichment in the first gigayear of cosmic time (e.g. Barth et al. 2003; Maiolino et al. 2003; Jiang et al. 2007; Kurk et al. 2007). Their absorption spectra show that the intergalactic medium (IGM) at  $z \sim 6$  is close to the reionization epoch (e.g. Becker et al. 2001; Djorgovski et al. 2001; Fan et al. 2006b,c).

The majority of the currently known  $z \sim 6$  quasars were discovered from  $\sim 8000$  deg<sup>2</sup> of imaging data of the Sloan Digital Sky Survey (SDSS; York et al. 2000). They were selected as *i*-dropout objects using optical colors. Several other high-redshift quasars were discovered based on their infrared or radio emission. For example, Cool et al. (2006) discovered one quasar at  $z = 5.85$  in the NOAO Deep Wide-Field Survey (NDWFS; Jannuzi & Dey 1999) Bootes Field using the AGN and Galaxy Evolution Survey (AGES) spectroscopic observations. The quasar was selected from a *Spitzer* mid-infrared quasar sample and has a  $z_{AB}$  magnitude of 20.68 and an optical luminosity of  $M_B = -26.52$ . By matching the FLAMINGOS Extragalactic Survey IR survey (Elston et al. 2006) data to the Faint Images of the Radio Sky at Twenty-cm (FIRST; Becker et al. 1995) data, McGreer et al. (2006) discovered a radio-loud quasar at  $z = 6.12$  in 4 deg<sup>2</sup> of the NDWFS region. This quasar is a broad absorption line (BAL) quasar with an optical luminosity of  $M_B = -26.9$ , comparable to the luminous SDSS quasars at  $z \sim 6$ .

Despite the high-redshift quasar surveys mentioned above, very little is known about faint quasars ( $z_{AB} > 20$ ) at  $z \sim 6$ . The SDSS main survey only probes the

Based on observations obtained with the Sloan Digital Sky Survey, which is owned and operated by the Astrophysical Research Consortium; the MMT Observatory, a joint facility of the University of Arizona and the Smithsonian Institution; the 6.5 meter Magellan Telescopes located at Las Campanas Observatory, Chile; the W.M. Keck Observatory, which is operated as a scientific partnership among the California Institute of Technology, the University of California and the National Aeronautics and Space Administration, and was made possible by the generous financial support of the W.M. Keck Foundation.

<sup>1</sup> Steward Observatory, University of Arizona, 933 North Cherry Avenue, Tucson, AZ 85721

<sup>2</sup> Fermi National Accelerator Laboratory, P.O. Box 500, Batavia, IL 60510

<sup>3</sup> Physics Department, University of California, Davis, CA 95616

<sup>4</sup> Institute of Geophysics and Planetary Physics, Lawrence Livermore National Laboratory, Livermore, CA 94550

<sup>5</sup> Space Telescope Science Institute, 3700 San Martin Drive, Baltimore, MD 21218

<sup>6</sup> School of Physics, University of Exeter, Stocker Road, Exeter EX4 4QL, UK

<sup>7</sup> Department of Astrophysical Sciences, Princeton University, Princeton, NJ 08544

<sup>8</sup> Department of Physics, Drexel University, 3141 Chestnut Street, Philadelphia, PA 19104

<sup>9</sup> Max-Planck-Institut für Astronomie, Königstuhl 17, D-69117 Heidelberg, Germany

<sup>10</sup> Department of Astronomy and Astrophysics, Pennsylvania State University, 525 Davey Laboratory, University Park, PA 16802

most luminous quasars, and with a density of  $1/470 \text{ deg}^2$  (Fan et al. 2006a). The Cool et al. (2006) quasar at  $z = 5.85$  was  $z_{AB} > 20$ , but the sample contains a single object and is selected from an area of less than  $10 \text{ deg}^2$ . Mahabal et al. (2005) found a very faint quasar with  $z_{AB} = 23.0$  at  $z = 5.70$  in a  $2.5 \text{ deg}^2$  field around the luminous quasar SDSS J114816.64+525150.3<sup>11</sup> at  $z = 6.42$ . Willott et al. (2005) imaged a  $3.83 \text{ deg}^2$  region down to  $z_{AB} = 23.35$  in the first results of the Canada-France High-redshift Quasar Survey (CFHQS) and did not find any quasars at  $z > 5.7$ . In these surveys both the quasar samples and the survey areas are very small, thus they do not provide a good statistical study of high-redshift quasars at  $z_{AB} > 20$ . Recently, Willott et al. (2007) discovered four quasars at  $z > 6$  from about  $400 \text{ deg}^2$  of the CFHQS, including the most distant known quasar at  $z = 6.43$ . Three of these quasars have  $z_{AB}$  magnitudes fainter than 21. Since their follow-up observations are not yet complete, they did not determine the spatial density of these quasars.

Finding faint quasars at  $z \sim 6$  is important for studying the evolution of the quasar population and quasars' impact on their environments. Fan et al. (2004) obtained the bright-end quasar luminosity function (QLF) at  $z \sim 6$ , but the slope,  $-3.2 \pm 0.7$ , was very uncertain due to the small luminosity range of the sample. Richards et al. (2004) put a broad constraint on the bright-end slope of  $> -4.63$  ( $3\sigma$ ) from the absence of lenses in four quasars at  $z \sim 6$ . Shankar & Mathur (2007) have considered the implications of all existing  $z \sim 6$  quasar observations, including deep X-ray surveys, for the faint end of the high-redshift QLF. Based predominantly on the X-ray surveys, they argue that there is a flattening of the QLF at  $M_{1450} \gtrsim -24.67$ .

With the discovery of faint high-redshift quasars, the QLF can be well determined. The QLF at  $z \sim 6$  is important to understand BH growth at early epochs (e.g. Volonteri & Rees 2006; Wyithe & Padmanabhan 2006). While bright quasars at high redshift have central BH masses between  $10^9$  and  $10^{10} M_\odot$ , fainter quasars with  $z_{AB} > 20$  are expected to harbor BHs with masses of a few times  $10^8 M_\odot$  or below (e.g. Kurk et al. 2007), which may be associated with galaxies of lower masses. The QLF also enables us to determine the quasar contribution to the UV background at  $z \sim 6$ . Detection of complete Gunn-Peterson troughs (Gunn & Peterson 1965) among the highest-redshift quasars indicates a rapid increase of the IGM neutral fraction at  $z \sim 6$ , and suggests that we have reached the end of the reionization epoch (e.g. Becker et al. 2001; Djorgovski et al. 2001; Fan et al. 2006c). It is unclear what individual contributions of galaxies and quasars to the reionization are. Although there is evidence showing that quasars are probably not the main contributor to reionization (e.g. Salvaterra et al. 2007; Srbinsky & Wyithe 2007; Shankar & Mathur 2007), a proper determination of the QLF at  $z \sim 6$  is needed to constrain the the quasar contribution.

In this paper we present the discovery of five  $z \sim 6$  quasars with  $20 < z_{AB} < 21$  selected from  $260 \text{ deg}^2$  of the

SDSS southern survey, a deep imaging survey obtained by repeatedly scanning a  $300 \text{ deg}^2$  area in the Fall Celestial Equatorial Stripe (Adelman-McCarthy et al. 2007a). One of the five quasars, SDSS J020332.39+001229.3 (hereafter SDSS J0203+0012), was independently discovered by matching the UKIRT Infrared Deep Sky Survey (UKIDSS; Warren et al. 2007) data to the SDSS data (Venemans et al. 2007). These five quasars, together with another quasar, SDSS J000552.34-000655.8 (hereafter SDSS J0005-0006) previously discovered in this region (Fan et al. 2004), form a well-defined low-luminosity quasar sample at high redshift. We use this sample and the luminous SDSS quasar sample to measure the QLF and constrain the quasar contribution to the reionization of the universe at  $z \sim 6$ .

The structure of the paper is as follows. In § 2 we introduce the quasar selection criteria and photometric and spectroscopic observations of quasar candidates. In § 3 we describe the properties of the five new quasars. We derive the QLF at  $z \sim 6$  in § 4, and discuss the contribution of quasars to the ionizing background in § 5. We give a brief summary in § 6. Throughout the paper we use a  $\Lambda$ -dominated flat cosmology with  $H_0 = 70 \text{ km s}^{-1} \text{ Mpc}^{-1}$ ,  $\Omega_m = 0.3$ , and  $\Omega_\Lambda = 0.7$  (Spergel et al. 2007).

## 2. CANDIDATE SELECTION AND OBSERVATION

### 2.1. SDSS Deep Imaging Data

The SDSS is an imaging and spectroscopic survey of the sky (York et al. 2000) using a dedicated wide-field  $2.5 \text{ m}$  telescope (Gunn et al. 2006) at Apache Point Observatory. Imaging is carried out in drift-scan mode using a  $142 \text{ mega-pixel}$  camera (Gunn et al. 1998) which gathers data in five broad bands, *ugriz*, spanning the range from  $3000$  to  $10,000 \text{ \AA}$  (Fukugita et al. 1996), on moonless photometric (Hogg et al. 2001) nights of good seeing. The effective exposure time is  $54$  seconds. The images are processed using specialized software (Lupton et al. 2001), and are photometrically (Tucker et al. 2006; Ivezić et al. 2004) and astrometrically (Pier et al. 2003) calibrated using observations of a set of primary standard stars (Smith et al. 2002) on a neighboring  $20\text{-inch}$  telescope. All magnitudes are roughly on an AB system (Oke & Gunn 1983), and use the asinh scale described by Lupton et al. (1999).

A primary goal of the SDSS imaging survey is to scan  $8500 \text{ deg}^2$  of the north Galactic cap (hereafter referred to as the SDSS main survey). In addition to the main survey, SDSS also conducts a deep survey by repeatedly imaging a  $300 \text{ deg}^2$  area on the Celestial Equator in the south Galactic cap in the Fall (hereafter referred to as the SDSS deep survey; Adelman-McCarthy et al. 2007a). This deep stripe (also called Stripe 82) spans  $20^{\text{h}} < \text{RA} < 4^{\text{h}}$  and  $-1.25^\circ < \text{Dec} < 1.25^\circ$ . The multi-epoch images, when coadded, allow the selection of much fainter quasars than the SDSS main survey. Jiang et al. (2006b) have used the deep data to find low-redshift faint quasars selected from the SDSS coadded catalog, i.e., each run goes through the photometric pipeline PHOTO separately, and the resulting catalogs are coadded. The SDSS deep survey will eventually reach a depth of  $i_{AB} = 24.0 \sim 24.5$  ( $5 \sigma$  detection for point sources) with more than  $50$  epochs

<sup>11</sup> The naming convention for SDSS sources is SDSS JHHMMSS.SS±DDMMSS.S, and the positions are expressed in J2000.0 coordinates. We use SDSS JHHMM±DDMM for brevity.

of data (Adelman-McCarthy et al. 2007b). The area and the depth will then be comparable to the CFHQS, which has covered  $\sim 400 \text{ deg}^2$  to a limit of  $i_{AB} \sim 24.5$  (Willott et al. 2007).

At the time the coadded images used in this paper were made, 2005, a given area of sky on Stripe 82 had been scanned 5–18 times under standard SDSS imaging conditions, and all available data were included in this version of the coadds. The construction of the coadds is summarized as follows. First, each input image was calibrated to a standard SDSS zeropoint using the median of the SDSS photometric solutions for the runs covering the area. For each image we made an inverse variance image to serve as a weight map, and within the map we assigned near-zero values to pixels with the INTERP bit set in the fpMask files of PHOTO, which indicates that a bad pixel, bad column, or cosmic ray has been interpolated over. After the images were sky subtracted using the PHOTO sky estimate, each image was mapped onto a uniform rectangular output astrometric grid using a modified version of the registration software SWARP (Bertin et al. 2002). The main modification was to incorporate the known SDSS camera distortions into the astrometry. The weight maps were subjected to the same mapping. The mapping used the LANCZOS3 kernel for the images and weights, while the INTERP bit images were mapped using NEAREST before being used to set near-zero values in the weight map images. The mapped images were then coadded using a flux scaled inverse-variance weighted average. The resulting images had known photometric and astrometric calibrations. For precision photometry, the PSFs as a function of position on the images were required. We used an algorithm (implemented in PHOTO) that coadded the PSFs as a function of position known from each input image using the same weights as the images were averaged. Once the photometry, astrometry, and PSF were known, we proceeded to run a version of FRAMES (the main portion of PHOTO) slightly modified to take effective gains and sky noises into account when calculating error estimates. The uncalibrated output of PHOTO was adjusted and placed on the SDSS AB system using a slightly modified version of the SDSS target selection software TARGET. The details of the construction of the coadds will be left for a forthcoming paper.

The resulting data were tested in three ways. First, object by object comparisons were made against single-run SDSS data. Second, object by object comparisons were made with the SDSS coadded catalogs produced by suitably averaging all the catalog information from the individual runs covering Stripe 82 (courtesy of R. Scranton and D. Johnston). Third, statistical internal measurements, such as stellar color-color diagrams, were made. These tests show that the images were properly coadded and the depth of the coadds is close to what was expected from standard error propagation. Figure 1 compares the photometric errors of PSF magnitudes for point sources in the SDSS main survey data and the SDSS coadded data. The error estimates were produced by the SDSS photometric pipeline PHOTO. From Figure 1 the photometric errors in the coadded data are significantly smaller than those in the single-run data.

In this paper we used the data in the range  $310^\circ < \text{RA} < 60^\circ$ , as there were significantly fewer than 10 runs

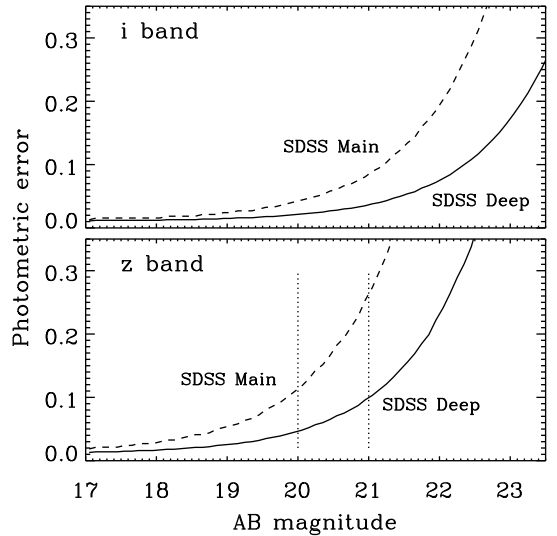


FIG. 1.— Photometric errors of PSF magnitudes for point sources as a function of  $i_{AB}$  and  $z_{AB}$  magnitudes. The error estimates were produced by the SDSS photometric pipeline PHOTO. The errors in the SDSS main coadded data are significantly smaller than those in the SDSS main survey data. They are close to those expected from  $\sigma_{\text{single}}/N_{\text{epoch}}^{1/2}$ , where  $\sigma_{\text{single}}$  is the error in SDSS single-run data and  $N_{\text{epoch}}$  is the number of the runs used in the coadds. The flux limits of the  $z \sim 6$  quasar surveys used in the SDSS main survey (e.g. Fan et al. 2001a) and in our work are indicated as the two vertical dotted lines, at which  $\sigma(z_{AB}) \sim 0.1$ .

covering the range  $300^\circ < \text{RA} < 310^\circ$ . The data also contains some “holes” in which the coadded images were not available. The effective area for this work is  $260 \text{ deg}^2$ . The median seeing as measured in the *riz* bands was  $1.2'' \pm 0.05''$ , where the error is the standard deviation of the seeing measured by PHOTO across the coadded images on Stripe 82.

## 2.2. Quasar Selection Procedure

Because of the rarity of high-redshift quasars and overwhelming number of contaminants, our selection procedure of  $z > 5.7$  faint quasars from the multi-epoch SDSS imaging data contains the following separate steps (see also Fan et al. 2001a, 2003).

1. Select *i*-dropout sources from the SDSS deep stripe. Objects with  $i_{AB} - z_{AB} > 2.2$  and  $z_{AB} < 21$  that were not detected in the *ugr* bands were selected as *i*-dropout objects. We rejected sources with one or more of the following SDSS processing flags: BRIGHT, EDGE, BLENDED, SATUR, MAYBE\_CR, and MAYBE\_EGHOST (see Stoughton et al. 2002). At  $z > 5.7$ , the Ly $\alpha$  emission line begins to move out of the SDSS *i* filter, so a simple cut of  $i_{AB} - z_{AB} > 2.2$  is used to separate high-redshift quasars (and cool brown dwarfs) from the majority of stellar objects (e.g. Fan et al. 2001a). At  $z_{AB} = 21$ , the photometric errors of the coadded data reach  $\sigma(z_{AB}) \sim 0.1$  as shown in Figure 1, so the  $z_{AB} < 21$  criterion guarantees a high quasar selection efficiency due to small photometric errors.
2. Remove false *i*-dropout objects. All *i*-dropout objects were visually inspected, and false detections

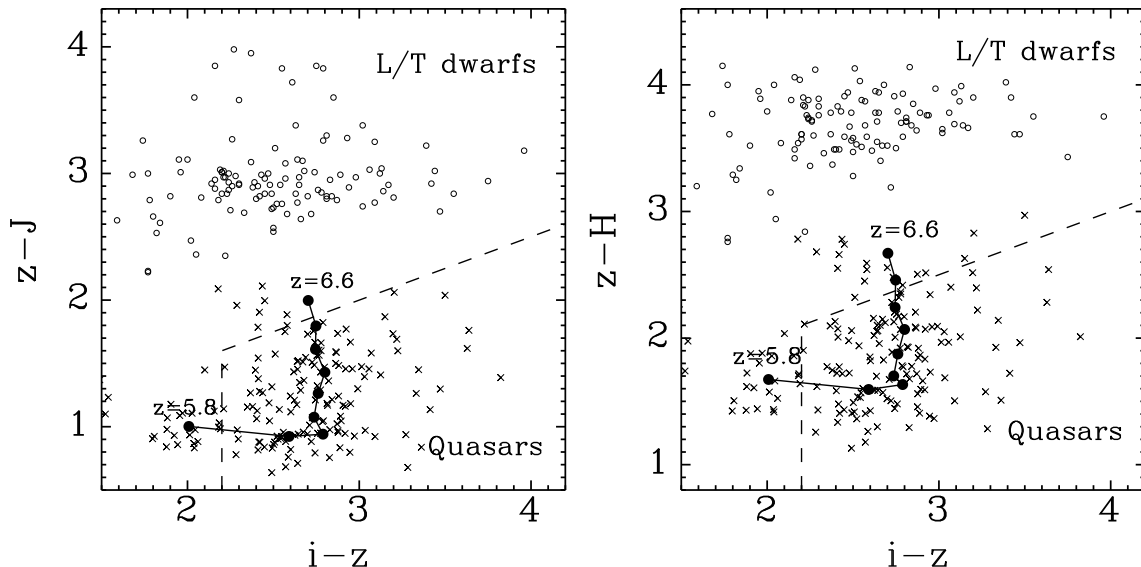


FIG. 2.— The  $i_{AB} - z_{AB}$  vs.  $z_{AB} - J$  (and  $H$ ) color-color diagrams. The open circles represent known L/T dwarfs from Golimowski et al. (2004), Knapp et al. (2004), and Chiu et al. (2006). The crosses represent simulated quasars at  $5.8 < z < 6.6$ . The median track of quasar colors as a function of redshift is shown as the filled circles. We use the dashed lines to separate high-redshift quasar candidates from L/T dwarfs. Note that in practice there is no unambiguous separation between the dwarf locus and the quasar locus due to photometric errors.

were deleted from the list of candidates. The majority of the contaminants are cosmic rays. Although the SDSS photometric pipeline effectively rejects cosmic rays, the leakage of a tiny fraction of cosmic rays will contribute a large contamination to our sample. Cosmic rays were recognized by comparing the individual multi-epoch images making up the coadds. Brown dwarfs with high proper motions can be removed in a similar way, since the multi-epoch images were taken over a period of five years. In the selection of luminous  $z \sim 6$  quasars in the SDSS main survey, Fan et al. (2001a) used an additional step,  $z$ -band photometry of  $i$ -dropout objects, to eliminate cosmic rays and improve the photometry of potential candidates. In this work we did not use this step, as the photometry of the coadds is robust. About 60  $i$ -dropout objects remained in this step.

3. Near-infrared (NIR) photometry of  $i$ -dropout objects. We then carried out NIR ( $J$  or  $H$  band) photometry of  $i$ -dropout objects selected from the previous step. The details of the NIR observations are described in § 2.3. Using the  $i_{AB} - z_{AB}$  vs.  $z_{AB} - J$  (or  $H$ ) color-color diagrams (Figure 2), high-redshift quasar candidates were separated from brown dwarfs (L and T dwarfs), which have more than ten times higher surface density. The open circles in Figure 2 represent known L/T dwarfs from Golimowski et al. (2004), Knapp et al. (2004), and Chiu et al. (2006). The crosses represent simulated quasars at  $5.8 < z < 6.6$ . Although there is no clear separation between the dwarf locus and the quasar locus due to photometric errors, we selected quasars with the following criteria,

$$i_{AB} - z_{AB} > 2.2 \ \&\& \ z_{AB} - J < 0.5(i_{AB} - z_{AB}) + 0.5, \quad (1)$$

$$\text{or } i_{AB} - z_{AB} > 2.2 \ \&\& \ z_{AB} - H < 0.5(i_{AB} - z_{AB}) + 1.0. \quad (2)$$

A total of 14 objects satisfied the criteria.

4. Follow-up spectroscopy of quasar candidates. The final step is to carry out optical spectroscopic observations of quasar candidates to identify high-redshift quasars. The details of the spectroscopic observations are described in § 2.3.

### 2.3. NIR Photometry and Optical Spectroscopic Observations

In the first two steps we described above, we selected about 60  $i$ -dropout objects with  $i_{AB} - z_{AB} > 2.2$  and  $z_{AB} < 21$  from 260 deg<sup>2</sup> of the SDSS coadded imaging data. After the selection of  $i$ -dropouts, we carried out  $J$  or  $H$ -band<sup>12</sup> photometry of these  $i$ -dropouts using the SAO Widefield InfraRed Camera (SWIRC) on the MMT in November 2005 and October 2006 to separate quasar candidates and cool dwarfs. We used a  $5 \times 5$  dither pattern to obtain good sky subtraction and to remove cosmic rays. The exposure time at each dither position was 30 seconds. The total exposure time for each target was calculated to achieve an uncertainty of  $\sigma_J$  (or  $\sigma_H$ )  $\sim 0.08$ . The typical exposure time on individual targets is 10 minutes. The SWIRC data were reduced using standard IRAF<sup>13</sup> routines. Five bright objects from the Two Micron All Sky Survey (2MASS; Skrutskie et al. 2006) in the field of each target were used to apply the aperture correction and absolute flux calibration.

After the NIR photometry of the  $i$ -dropouts, we selected quasar candidates that satisfied the criteria of Equation 1 or 2. Optical spectroscopy of the candidates was carried out using the Echelle Spectrograph and Imager (ESI; Sheinis et al. 2002) on the Keck-II in January 2006 and the Low Dispersion Survey Spectrograph

<sup>12</sup> The  $J$ -band photometry is more efficient for selecting  $z \sim 6$  quasars. Due to an instrument problem, however, the filter wheel was stuck and only the  $H$  filter was available on the night of October 2006.

<sup>13</sup> IRAF is distributed by the National Optical Astronomy Observatories, which are operated by the Association of Universities for Research in Astronomy, Inc., under cooperative agreement with the National Science Foundation.

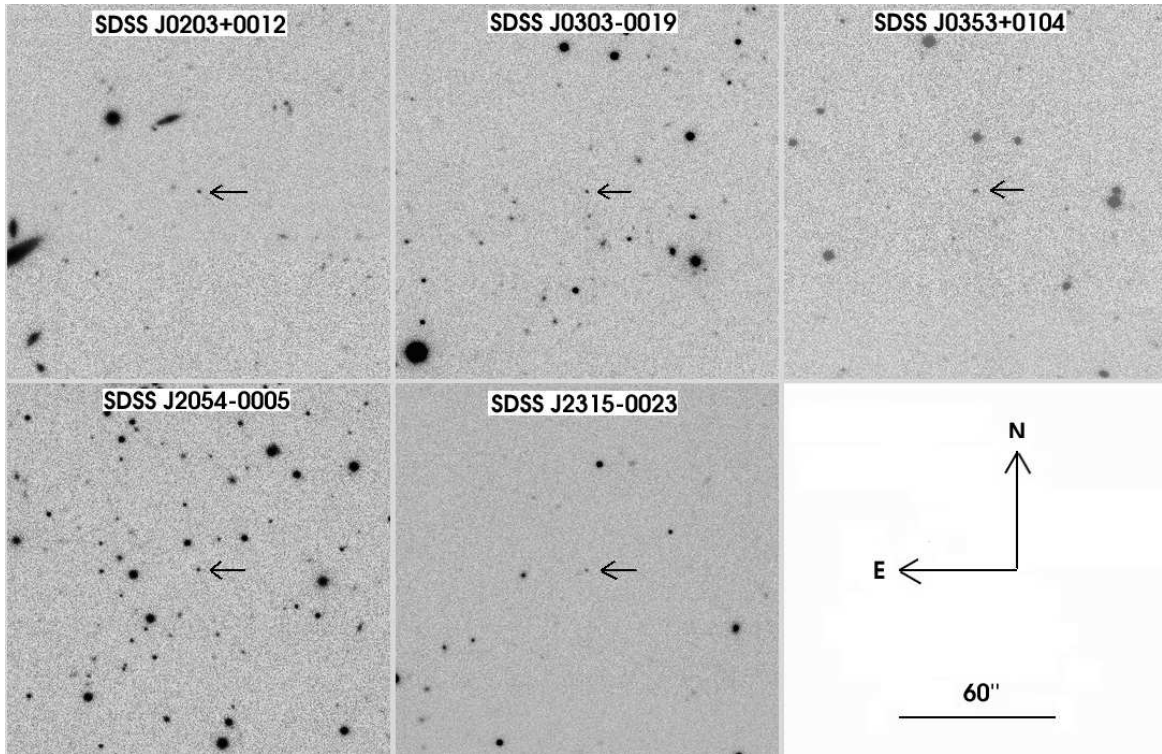


FIG. 3.— The  $z$ -band finding charts of the five new  $z \sim 6$  quasars discovered in the SDSS deep stripe.

TABLE 1  
OPTICAL AND NIR PHOTOMETRY

Quasar (SDSS)	Redshift <sup>a</sup>	$i_{AB}$ (mag)	$z_{AB}$ (mag)	$J$ (mag)	$H$ (mag)
J000552.34–000655.8 <sup>b</sup>	$5.850 \pm 0.003$	$23.40 \pm 0.34$	$20.54 \pm 0.10$	$19.87 \pm 0.10$	...
J020332.39+001229.3 <sup>c</sup>	$5.854 \pm 0.002$	$23.72 \pm 0.22$	$20.87 \pm 0.10$	$19.05 \pm 0.08$	...
J030331.40–001912.9	$6.070 \pm 0.001$	$23.92 \pm 0.23$	$20.85 \pm 0.07$	...	$19.46 \pm 0.10$
J035349.72+010404.4	$6.049 \pm 0.004$	$24.03 \pm 0.30$	$20.54 \pm 0.08$	...	$18.55 \pm 0.06$
J205406.49–000514.8	$6.062 \pm 0.004$	$23.30 \pm 0.22$	$20.72 \pm 0.09$	$19.18 \pm 0.06$	...
J231546.57–002358.1	$6.117 \pm 0.006$	$24.90 \pm 0.28$	$20.88 \pm 0.08$	$19.94 \pm 0.08$	...

NOTE. — The  $i_{AB}$  and  $z_{AB}$  magnitudes are AB magnitudes and the  $J$  and  $H$  magnitudes are Vega-based magnitudes.

<sup>a</sup> The errors of the redshifts are the uncertainties obtained from our fitting process.

<sup>b</sup> This quasar was discovered by Fan et al. (2004). The magnitudes were taken from Fan et al. (2004), and the redshift was determined from the Mg II emission line by Kurk et al. (2007).

<sup>c</sup> This quasar was independently discovered by Venemans et al. (2007).

(LDSS-3) on Magellan-II in October 2006. The observations on ESI were performed in echellette mode, which provides excellent sensitivity from 4000 to 10,000 Å. The observations on LDSS-3 were performed in longslit mode. LDSS-3 was designed to be very red sensitive. We used the VPH red grism with a ruling density of 660 lines/mm. The VPH red grism offers excellent throughput in the wavelength range from 6000 to 10,000 Å. The exposure time for each target was 20 minutes, which is sufficient to identify  $z \sim 6$  quasars in our sample. If a target was identified as a quasar, several further exposures were taken to improve the spectral quality. The quasar data were reduced using standard routines. After bias subtraction, flat-fielding, and wavelength calibration were applied to the frames, one-dimensional spectra were extracted, and were flux calibrated using the spectra of spectroscopic standard stars.

### 3. DISCOVERY OF FIVE NEW QUASARS AT $Z \sim 6$

From the spectroscopic observations on Keck/ESI and Magellan/LDSS-3 we discovered five  $z \sim 6$  quasars in the SDSS deep stripe. Their  $z$ -band finding charts are shown in Figure 3. Note that SDSS J0203+0012 was independently discovered by Venemans et al. (2007). Another  $z \sim 6$  quasar in this area, SDSS J0005–0006 discovered by Fan et al. (2004), was recovered by our selection criteria. These six quasars comprise a complete flux-limited sample at  $z_{AB} < 21$ . The optical and NIR properties of the quasars are given in Table 1. The  $i_{AB}$  and  $z_{AB}$  magnitudes of the newly discovered quasars are taken from the SDSS deep imaging data, and their  $J$  and  $H$  magnitudes are obtained from our MMT/SWIRC observations. All the quasars have  $z_{AB}$  magnitudes between 20 and 21. The surface density of  $z \sim 6$  quasars with  $z_{AB} < 20$  is

about  $1/470 \text{ deg}^2$  (Fan et al. 2006a), so it is reasonable to find no quasars with  $z_{AB} < 20$  in a  $260 \text{ deg}^2$  area.

The optical spectra of the six quasars are shown in Figure 4. The spectrum of SDSS J0005–0006 was taken from Fan et al. (2004). The spectra of SDSS J035349.72+010404.4 (hereafter SDSS J0353+0104) and SDSS J231546.57–002358.1 (hereafter SDSS J2315–0023) were taken on Keck/ESI with a total exposure time of 60 minutes on each source. The spectra of the other three quasars were obtained with Magellan/LDSS-3, and the total exposure time on each source was 100 minutes. Each spectrum shown in Figure 4 has been scaled to the corresponding  $z_{AB}$  magnitude given in Table 1, thereby placed on an absolute flux scale.

We estimate the redshifts for the new quasars from either the Ly $\alpha$ , N v  $\lambda 1240$  (hereafter N v), or the O I  $\lambda 1304$  (hereafter O I) emission line. For each quasar, we measure the line center of one strong emission line using a Gaussian profile to fit the top  $\sim 50\%$  of the line. This provides a rough estimate of the redshift. Using this redshift we subtract the power-law continuum and decompose the blended Ly $\alpha$  and N v emission lines into individual components. The details are described in the next paragraph. Then we determine the redshifts from individual emission lines. The redshift of SDSS J030331.40–001912.9 (hereafter SDSS J0303–0019) is measured from the N v emission line, which is well separated from Ly $\alpha$  due to the narrow line width. The measured redshift  $6.070 \pm 0.001$  is consistent with the redshift  $6.069 \pm 0.002$  determined from the weak O I emission line. SDSS J0353+0104 is a BAL quasar as seen from strong absorption features around Ly $\alpha$ , so its redshift is measured from the O I emission line. The redshifts of the other three quasars are estimated from the Ly $\alpha$  emission lines. They are usually biased because the blue side of Ly $\alpha$  is affected by the Ly $\alpha$  forest absorption (Schneider et al. 1991). The mean shift with respect to the systemic redshift at  $z > 3$  is about  $600 \text{ km s}^{-1}$  (Shen et al. 2007), corresponding to  $\delta z \sim 0.015$  at  $z \sim 6$ . We correct for this bias for the redshifts measured from Ly $\alpha$ . The results are listed in Column 2 of Table 1. The errors in the table are the uncertainties obtained from our fitting process. For the redshifts measured from Ly $\alpha$ , their real errors could be much larger due to the scatter in the relation between Ly $\alpha$  redshifts and systemic redshifts (Shen et al. 2007). In our sample four quasars have redshifts greater than 6. The most distant quasar, SDSS J2315–0023, is at  $z = 6.12$ .

We measure the rest-frame equivalent width (EW) and full width at half maximum (FWHM) of Ly $\alpha$  and N v for each quasar except the BAL quasar SDSS J0353+0104. To allow the analysis of the emission lines we first fit and subtract the continuum. The wavelength coverage of each spectrum is too short to fit the continuum slope, so we assume it is a power law with a slope  $\alpha_\nu = -0.5$  ( $f_\nu \sim \nu^{\alpha_\nu}$ ), and normalize it to the spectrum at rest frame 1275–1295 Å, a continuum window with little contribution from line emission. Ly $\alpha$  and N v are usually blended with each other, so we use three Gaussian profiles to simultaneously fit the two lines, with the first two profiles representing broad and narrow components of Ly $\alpha$  and the third representing N v. Since the blue side of the Ly $\alpha$  emission line is strongly absorbed by

Ly $\alpha$  forest absorption systems, we only fit the red side of the line and assume that the line is symmetric. We ignore the weak Si II  $\lambda 1262$  emission line on the red side of N v. The measured EW and FWHM in units of Å are shown in Table 2. We also give the FWHM of Ly $\alpha$  in units of  $\text{km s}^{-1}$ . We emphasize that the EW and FWHM of Ly $\alpha$  in the table have taken into account the absorbed emission by the Ly $\alpha$  forest, while most previous studies did not take this absorption into account.

The distributions of the Ly $\alpha$  EW and FWHM are broad. The average Ly $\alpha$  EW and FWHM measured from the low-redshift SDSS composite spectrum of Vanden Berk et al. (2001) are about  $90 \text{ Å}$  and  $20 \text{ Å}$  ( $\sim 5000 \text{ km s}^{-1}$ ), respectively. The EW of Ly $\alpha$ +N v from a sample of quasars at  $3.6 < z < 5.0$  is  $69 \pm 18 \text{ Å}$  (Fan et al. 2001b), although this is affected by the Ly $\alpha$  forest absorption. We analyzed a sample of 20 luminous SDSS quasars at  $z \sim 6$ , and find that the mean Ly $\alpha$  EW and FWHM are  $56 \text{ Å}$  and  $25 \text{ Å}$  (also corrected for the Ly $\alpha$  forest absorption) with large scatters of  $40 \text{ Å}$  and  $11 \text{ Å}$ , respectively. In Table 2, three of our quasars (SDSS J0005–0006, SDSS J0303–0019, and SDSS J2315–0023) have Ly $\alpha$  FWHM less than half of the typical value. The Ly $\alpha$  FWHM in both SDSS J0005–0006 and SDSS J0303–0019 is only  $\sim 1600 \text{ km s}^{-1}$ . However, their EW are close to or stronger than the typical Ly $\alpha$  EW. On the contrary, the other two quasars, SDSS J0203+0012 and SDSS J205406.49–000514.8 (hereafter SDSS J2054–0005), have typical Ly $\alpha$  FWHM, but very weak Ly $\alpha$  EW.

The best-fitting power-law continuum is also used to calculate  $m_{1450}$  and  $M_{1450}$ , the apparent and absolute AB magnitudes of the continuum at rest-frame 1450 Å. The results are given in Table 3. The sample spans a luminosity range of  $-26.5 \leq M_{1450} \leq -25.4$ . Because the Ly $\alpha$  emission usually consists of a large fraction of the total emission in the  $z$ -band spectra of these quasars, the large scatter in the Ly $\alpha$  EW results in a large scatter in the distributions of  $m_{1450}$  and  $M_{1450}$ , even though the  $z_{AB}$  magnitudes lie in the small range  $20.5 < z_{AB} < 20.9$ .

### 3.1. Notes on individual objects

**SDSS J0005–0006** ( $z = 5.850$ ). SDSS J0005–0006 was discovered by Fan et al. (2004). This quasar has a very narrow Ly $\alpha$  emission line. The rest-frame FWHM of Ly $\alpha$  is only  $1680 \text{ km s}^{-1}$  (after corrected for the Ly $\alpha$  forest absorption). The strong N v emission line is well separated from Ly $\alpha$ . The central BH mass is  $3 \times 10^8 M_\odot$  (Kurk et al. 2007), an order of magnitude lower than the BH masses in luminous quasars at  $z \sim 6$  (e.g. Barth et al. 2003; Vestergaard 2004; Jiang et al. 2007; Kurk et al. 2007). SDSS J0005–0006 was marginally detected in the *Spitzer* IRAC  $8.0\mu\text{m}$  band and was not detected in the *Spitzer* MIPS  $24\mu\text{m}$  band, indicating that there is no hot dust emission in this quasar (Jiang et al. 2006a).

**SDSS J0203+0012** ( $z = 5.854$ ). SDSS J0203+0012 was independently discovered by matching the UKIDSS data to the SDSS data (Venemans et al. 2007). Its Ly $\alpha$  emission line is broad but weak. The Ly $\beta$  and O VI  $\lambda 1033$  (hereafter O VI) emission lines are clearly seen at  $\sim 7000 \text{ Å}$ . A C IV  $\lambda\lambda 1548, 1550$  absorption doublet is detected at  $\lambda\lambda = 8480.1, 8494.3 \text{ Å}$ ; this was also noticed by Venemans et al. (2007).

**SDSS J0303–0019** ( $z = 6.070$ ). SDSS J0303–0019

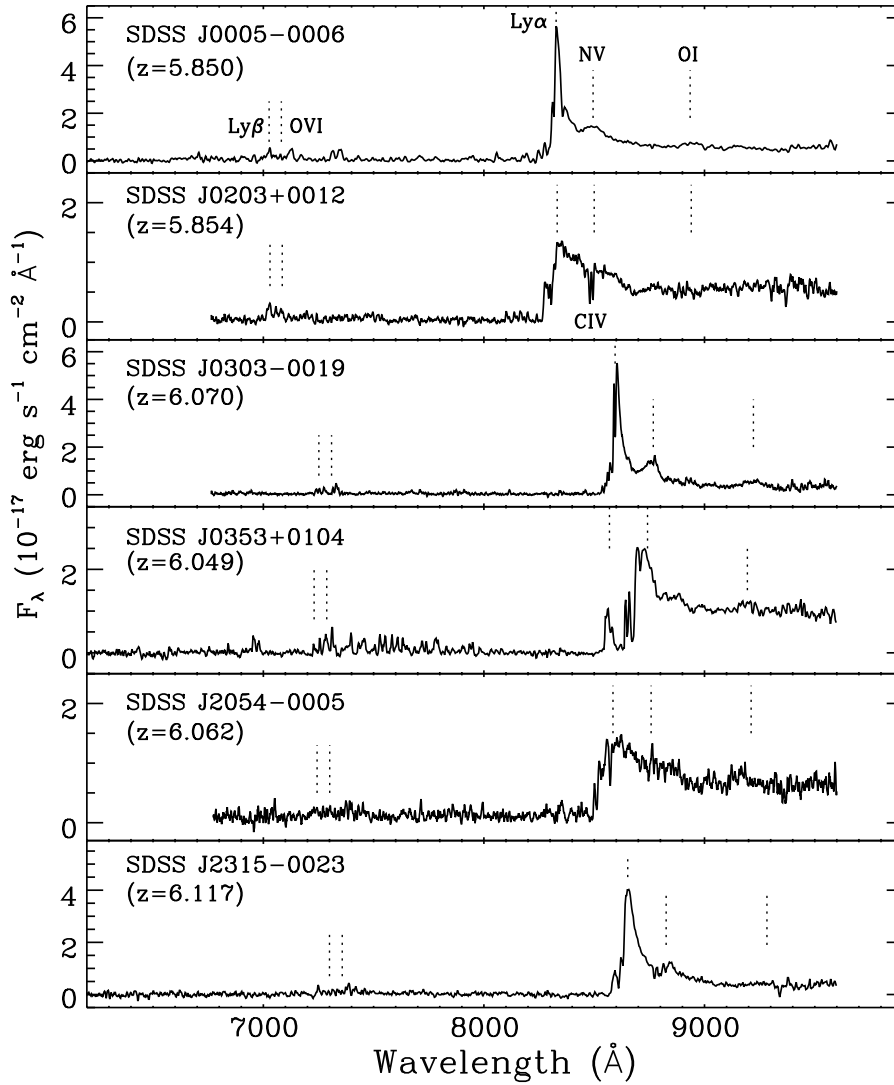


FIG. 4.— Optical spectra of the six high-redshift quasars discovered in the SDSS deep stripe. The spectra of SDSS J0005–0006, SDSS J0353+0104, and SDSS J2315–0023 were taken on Keck/ESI with a total exposure time of 60 minutes on each source. The spectra of the other three quasars were taken on Magellan/LDSS-3 with a total exposure time of 100 minutes on each source. The ESI spectra have been binned by 10 pixels and the LDSS-3 spectra been smoothed by 5 pixels. Four quasars in this sample are at  $z > 6$ . Three quasars have narrow Ly $\alpha$  emission lines. SDSS J0353+0104 is a BAL quasar.

TABLE 2  
PROPERTIES OF THE LY $\alpha$  AND N V EMISSION LINES

Quasar (SDSS)	Redshift	EW (Ly $\alpha$ )	FWHM (Ly $\alpha$ )	EW (N v)	FWHM (N v)
J0005–0006	5.850	81.5 $\pm$ 2.5	6.8 $\pm$ 0.4 (1680 km s $^{-1}$ )	25.0 $\pm$ 1.0	18.9 $\pm$ 0.6
J0203+0012	5.854	35.9 $\pm$ 1.5	31.0 $\pm$ 2.4 (7650 km s $^{-1}$ )	8.1 $\pm$ 0.5	20.6 $\pm$ 0.9
J0303–0019	6.070	139.4 $\pm$ 2.4	6.4 $\pm$ 0.5 (1580 km s $^{-1}$ )	24.4 $\pm$ 0.6	9.9 $\pm$ 0.2
J0353+0104 <sup>a</sup>	6.049	...	...	...	...
J2054–0005	6.062	17.0 $\pm$ 1.1	19.4 $\pm$ 3.8 (4890 km s $^{-1}$ )	12.8 $\pm$ 0.7	30.8 $\pm$ 1.4
J2315–0023	6.117	126.8 $\pm$ 3.2	9.8 $\pm$ 0.5 (2420 km s $^{-1}$ )	37.4 $\pm$ 1.4	17.7 $\pm$ 0.7

NOTE. — Rest-frame FWHM and EW are in units of  $\text{\AA}$ . The EW and FWHM of the Ly $\alpha$  emission lines have been corrected for Ly $\alpha$  forest absorption.

<sup>a</sup> This is a BAL quasar, so we did not measure its emission line properties.

TABLE 3  
CONTINUUM PROPERTIES OF THE QUASARS

Quasar (SDSS)	Redshift	$m_{1450}$ (mag)	$M_{1450}$ (mag)
J0005–0006	5.850	$20.83 \pm 0.10$	$-25.82 \pm 0.10$
J0203+0012	5.854	$20.94 \pm 0.10$	$-25.72 \pm 0.10$
J0303–0019	6.070	$21.28 \pm 0.07$	$-25.43 \pm 0.07$
J0353+0104	6.049	$20.22 \pm 0.08$	$-26.49 \pm 0.08$
J2054–0005	6.062	$20.60 \pm 0.09$	$-26.11 \pm 0.09$
J2315–0023	6.117	$21.34 \pm 0.08$	$-25.38 \pm 0.08$

also has a very narrow Ly $\alpha$  emission line. The rest-frame FWHM of Ly $\alpha$  is  $1580 \text{ km s}^{-1}$ , similar to the Ly $\alpha$  width of SDSS J0005–0006. The strong N V emission line is well separated from Ly $\alpha$ . The Ly $\beta$  and O VI emission lines are clearly detected at  $\sim 7300 \text{ \AA}$ . The continuum emission in this quasar is very weak. The absolute magnitude  $M_{1450}$  is  $-25.43$ , roughly two magnitudes fainter than the luminous SDSS quasars at  $z \sim 6$ .

**SDSS J0353+0104** ( $z = 6.049$ ). SDSS J0353+0104 is a BAL quasar, as seen from strong absorption features around the Ly $\alpha$  emission line. Its redshift was measured from O I. The fraction of BAL quasars in this small sample is one out of six, similar to the low-redshift fraction (Trump et al. 2006), although C IV observations may yield further BAL examples. The Ly $\beta$  and O VI emission lines are seen at  $\sim 7300 \text{ \AA}$ .

**SDSS J2054–0005** ( $z = 6.062$ ). SDSS J2054–0005 has a very weak Ly $\alpha$  emission line. The rest-frame EW of Ly $\alpha$  is only  $17.0 \text{ \AA}$ , significantly smaller than the typical EW. But the FWHM of Ly $\alpha$ ,  $\sim 30 \text{ \AA}$ , is similar to the mean value of Ly $\alpha$  FWHM.

**SDSS J2315–0023** ( $z = 6.117$ ). SDSS J2315–0023 is the most distant quasar in this sample. The properties of the Ly $\alpha$  and N V emission lines are similar to those of SDSS J0005–0006 and SDSS J0303–0019. It has a narrow but strong Ly $\alpha$  emission line. The rest-frame EW and FWHM of Ly $\alpha$  are  $127 \text{ \AA}$  and  $2420 \text{ km s}^{-1}$ , respectively. It also has a very strong N V emission line.

#### 4. QLF AT $Z \sim 6$

The six quasars presented in this paper provide a flux-limited quasar sample at  $z > 5.8$ . The survey area is  $260 \text{ deg}^2$  and the magnitude limit is  $z_{AB} = 21$ . In this section we calculate the spatial density of the  $z > 5.8$  quasars in the SDSS deep stripe, and combine this faint quasar sample with the SDSS bright quasar sample to derive the QLF at  $z \sim 6$ .

We use the selection function to correct the sample incompleteness due to the selection criteria we applied. The selection function is defined as the probability that a quasar with a given magnitude, redshift, and intrinsic spectral energy distribution (SED) meets our selection criteria. By assuming a distribution for the intrinsic SEDs, we calculate the average selection probability as a function of magnitude and redshift. To do this, we first calculate the synthetic distribution of quasar colors for a given  $(M_{1450}, z)$ , following the procedures in Fan (1999) and Fan et al. (2001a). Then we calculate the SDSS magnitudes from the model spectra and incorporate photometric errors into each band. For an object with given  $(M_{1450}, z)$ , we generate a database of model quasars with the same  $(M_{1450}, z)$ . The detection proba-

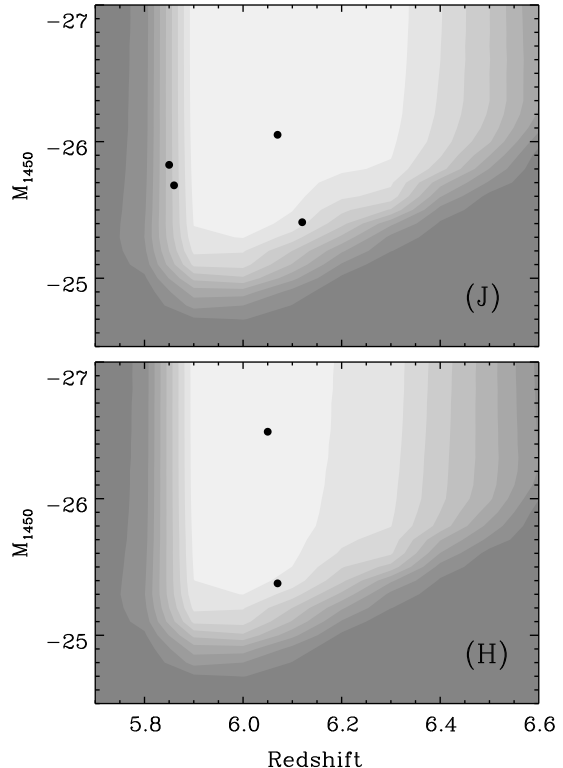


FIG. 5.— Quasar selection function as a function of  $M_{1450}$  and  $z$  for the two selection criterion equations (1a and 1b) based on  $J$  and  $H$  bands. The contours in the figure are selection probabilities from 0.9 to 0.1 with an interval of 0.1. The solid circles are the locations of the six  $z \sim 6$  quasars in our sample.

bility for this quasar is then the fraction of model quasars that meet the selection criteria. The details of the model and simulation are described in Fan (1999) and Fan et al. (2001a).

Figure 5 shows the selection function as a function of  $M_{1450}$  and  $z$  for the two selection criteria (Equations 1 and 2) based on  $J$  and  $H$  bands. The contours in the figure are selection probabilities from 0.9 to 0.1 with an interval of 0.1. The sharp decrease of the probability at  $z \sim 5.8$  is due to the color cut of  $i_{AB} - z_{AB} > 2.2$ . The two selection functions are slightly different. Due to smaller photometric errors in the  $i$  and  $z$  bands, our survey probes  $\sim 1.5$  magnitude deeper than the SDSS main survey (see Fan et al. 2001a). The solid circles are the locations of the six  $z \sim 6$  quasars. All the quasars have the selection probabilities greater than 0.5.

We derive the spatial density of the  $z > 5.8$  quasars using the traditional  $1/V_a$  method (Avni & Bahcall 1980). The available volume for a quasar with absolute magnitude  $M_{1450}$  and redshift  $z$  in a magnitude bin  $\Delta M$  and a redshift bin  $\Delta z$  is

$$V_a = \int_{\Delta M} \int_{\Delta z} p(M_{1450}, z) \frac{dV}{dz} dz dM, \quad (3)$$

where  $p(M_{1450}, z)$  is the selection function used to correct the sample incompleteness. We use one  $M_{1450}$ - $z$  bin for our small sample. The redshift integral is over the redshift range  $5.7 < z < 6.6$  and the magnitude integral is over the range that the sample covers. The spatial



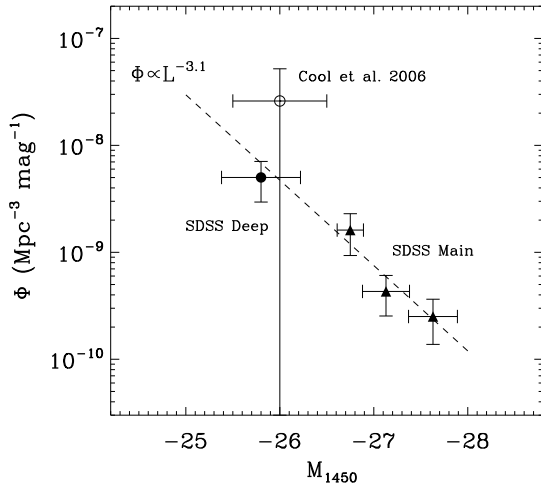


FIG. 6.— QLF at  $z \sim 6$ . The filled circle represents the density of the six quasars in the SDSS deep stripe and the filled triangles represent the densities from a study of 17 quasars from the SDSS main survey. The open circle is the constraint from the quasar discovered by Cool et al. (2006). The dashed line shows the best power-law fit to the SDSS quasars. The slope of the QLF is  $-3.1 \pm 0.4$ .

density and its statistical uncertainty can be written as

$$\rho = \sum_i \frac{1}{V_a^i}, \quad \sigma(\rho) = \left[ \sum_i \left( \frac{1}{V_a^i} \right)^2 \right]^{1/2}, \quad (4)$$

where the sum is over all quasars in the sample. This is similar to the revised  $1/V_a$  method of Page & Carrera (2000), since  $p(M_{1450}, z)$  has already corrected the incompleteness at the flux limit. We find that the spatial density at  $\langle z \rangle = 6.0$  and  $\langle M_{1450} \rangle = -25.8$  is  $\rho = (5.0 \pm 2.1) \times 10^{-9} \text{ Mpc}^{-3} \text{ mag}^{-1}$ .

In the SDSS main survey, more than 20 quasars at  $z > 5.8$  have been discovered. Seventeen of them were selected using similar criteria, and consist of a flux-limited quasar sample with  $z_{AB} < 20$ . This bright quasar sample includes 14 published quasars (e.g. Fan et al. 2006a) and three new quasars (Fan et al. in preparation). We combine this sample with our sample to derive the QLF at  $z \sim 6$ . The quasars in the combined sample are divided into four luminosity bins as shown in Figure 6. The QLF at the bright end at  $z \sim 6$  is well fit to a single power law  $\Phi(L_{1450}) \propto L_{1450}^\beta$ , or,

$$\Phi(M_{1450}) = \Phi^* 10^{-0.4(\beta+1)(M_{1450}+26)}, \quad (5)$$

where we only consider luminosity dependence and neglect redshift evolution over our narrow redshift range. The best fits are  $\Phi^* = (5.2 \pm 1.9) \times 10^{-9} \text{ Mpc}^{-3} \text{ mag}^{-1}$  and  $\beta = -3.1 \pm 0.4$ . The slope  $\beta = -3.1 \pm 0.4$  is consistent with the slope  $-3.2 \pm 0.7$  derived from the luminous sample alone by Fan et al. (2004) and with the slope  $> -4.63$  ( $3\sigma$ ) constrained by the lack of lenses in four high-redshift quasars (Richards et al. 2004).

## 5. DISCUSSION

We have derived the QLF at  $z \sim 6$  and found a steep slope ( $\beta = -3.1$ ) at the bright end. From the SDSS Data Release Three, Richards et al. (2006) showed strong evidence that the bright-end slope of the QLF significantly flattens from  $z \sim 2$  to 4. They found that the slope at

$z \sim 2.0$  is  $-3.1 \pm 0.1$  and the slope at  $z \sim 4.1$  flattens to  $-2.1 \pm 0.1$ . At  $z \sim 6$  the slope steepens again to  $-3.1 \pm 0.4$  at a significance level of  $\sim 2.5\sigma$ . The flattening of the slope at  $z \sim 4$  has been questioned by Fontanot et al. (2007), who argued that the spectral index Richards et al. (2006) used to correct for sample incompleteness was too blue. Hopkins et al. (2007) have analyzed the bolometric QLF from multiple surveys and stress that the flattening is seen at high significance. The lack of flattening claimed by Fontanot et al. (2007) would be real only if the distribution of quasar SEDs was redshift-dependent, contrary to what is found in most observations. Hence, the slope change from  $z \sim 4$  to  $z \sim 6$  is highly likely to be physical. The steepening of the slope at  $z \sim 6$  has important consequences in understanding early BH growth in quasars. Quasar evolution at  $z \sim 6$  is limited by the number of  $e$ -folding times available for BH accretion, therefore the shape of the QLF at  $z \sim 6$  puts strong constraints on models of BH growth (e.g. Wyithe & Loeb 2003; Hopkins et al. 2005; Volonteri & Rees 2006; Wyithe & Padmanabhan 2006; Li et al. 2007), and helps determine whether standard models of radiatively efficient Eddington accretion from stellar seeds are still allowed, or alternative models of BH birth (e.g. from intermediate-mass BHs) and BH accretion (super-Eddington or radiatively inefficient) are required (e.g. Volonteri & Rees 2006).

The steepening of the QLF slope also has a strong impact on the quasar contribution to the ionizing background at  $z \sim 6$ . The reionization of the universe occurs at  $z = 11 \pm 4$  (Spergel et al. 2007) and ends at  $z \sim 6$  (e.g. Fan et al. 2006b). Studies have shown that quasars/AGN alone are not likely to ionize the IGM at  $z \sim 6$  (e.g. Dijkstra et al. 2004; Meiksin 2005; Willott et al. 2005; Douglas et al. 2007; Salvaterra et al. 2007; Srinovskiy & Wyithe 2007; Shankar & Mathur 2007). Galaxies probably can provide enough photons for the reionization (e.g. Yan & Windhorst 2004; Bouwens et al. 2006; Kashikawa et al. 2006; McQuinn et al. 2007), however, the individual contributions of galaxies and quasars to the reionization are not well determined. The galaxy contribution is uncertain due to our lack of knowledge of factors such as the star-formation rate, the faint-end slope of the galaxy luminosity function, and the escape fraction of ionizing photons from galaxies (e.g. Bunker et al. 2004; Bouwens et al. 2006); while the quasar contribution is poorly constrained due to the lack of the knowledge of the faint end of the QLF at  $z \sim 6$ .

We estimate the rate at which quasars emit ionizing photons at  $z \sim 6$  from the QLF derived in § 4. Following Fan et al. (2001a), we calculate the photon emissivity of quasars per unit comoving volume at  $z \sim 6$  as

$$\dot{N}_q = \epsilon_{1450}^q n_{1450}^p, \quad (6)$$

where  $\epsilon_{1450}^q$  is the quasar emissivity at 1450 Å in units of  $\text{erg s}^{-1} \text{ Hz}^{-1} \text{ Mpc}^{-3}$  and  $n_{1450}^p$  is the number of ionizing photons for a source with a luminosity of  $1 \text{ erg s}^{-1} \text{ Hz}^{-1}$  at 1450 Å. We estimate  $\epsilon_{1450}^q$  from

$$\epsilon_{1450}^q = \int \Phi(M_{1450}) L_{1450} dM_{1450}, \quad (7)$$

where  $\Phi(M_{1450})$  is the QLF at  $z \sim 6$  and the integral is over the range  $-30 < M_{1450} < -16$ . At low redshift,

the shape of the QLF can be well modeled as a double power law with a steep bright end and a flat faint end (e.g. Boyle et al. 2000; Richards et al. 2005; Jiang et al. 2006b). At  $z \sim 6$ , we assume a double power-law form for the QLF as well,

$$\Phi(M_{1450}) = \frac{\Phi^*}{10^{0.4(\alpha+1)(M_{1450}-M_{1450}^*)} + 10^{0.4(\beta+1)(M_{1450}-M_{1450}^*)}}, \quad (8)$$

where  $\beta$  is the bright-end slope of the QLF,  $\alpha$  is the faint-end slope, and  $M_{1450}^*$  corresponds to the characteristic luminosity  $L_{1450}^*$ . At  $z \leq 2$ ,  $\alpha$  is roughly  $-1.6$  and  $M_{1450}^*$  is a function of redshift. Little is known about  $\alpha$  and  $M_{1450}^*$  at  $z > 4$ . At  $z \sim 6$ , the lower limit of  $M_{1450}^*$  is about  $-25$  as seen from Figure 6. Therefore we calculate  $\epsilon_{1450}^q$  for a range of  $\alpha$  between  $-1.2$  and  $-2.2$  and for a range of  $M_{1450}^*$  between  $-21$  and  $-25$ . The bright-end slope  $\beta$  is fixed to  $-3.1$  at the first step. We assume  $\Phi^*$  to be the value derived from Equation 5. This is a good approximation in the  $\alpha$  and  $M_{1450}^*$  ranges that we investigate here.

We calculate  $n_{1450}^p$  by assuming the quasar SED following

$$L_\nu \propto \begin{cases} \nu^{-0.5}, & \text{if } \lambda > 1050 \text{ \AA}; \\ \nu^{-1.8}, & \text{if } \lambda < 1050 \text{ \AA}, \end{cases} \quad (9)$$

and integrating the SED over an energy range of 1–4 Rydberg. The SED slope at  $\lambda > 1050 \text{ \AA}$  is taken from Vanden Berk et al. (2001) and at  $\lambda < 1050 \text{ \AA}$  from Zheng et al. (1997).

The total photon emissivity per unit comoving volume required to ionize the universe is estimated to be

$$\dot{N}_{ion}(z) = 10^{51.2} \text{ Mpc}^{-3} \text{ s}^{-1} \left(\frac{C}{30}\right) \times \left(\frac{1+z}{6}\right)^3 \left(\frac{\Omega_b h^2}{0.02}\right)^2 \quad (10)$$

(Madau et al. 1999), where baryon density  $\Omega_b h^2 = 0.02$  (Spergel et al. 2007) and  $C$  is the clumping factor of the IGM. We examine the effects of three values 1, 10, and 30 for  $C$ .

The results are shown in Figure 7(a). The solid lines represent the photon emissivity per unit comoving volume from quasars as a function of the faint-end slope  $\alpha$  and the characteristic luminosity  $M_{1450}^*$ . The dashed lines show the photon emissivity required to ionize the IGM at  $z \sim 6$  for  $C = 1$ ,  $C = 10$ , and  $C = 30$ , respectively. There is an uncertainty of  $0.4$  ( $1\sigma$ ) in the bright-end slope  $\beta$ , so we repeat our analysis for  $\beta = -3.5$ . The results are given in Figure 7(b). This figure shows that

1. The significance of the quasar contribution to the ionizing background at  $z \sim 6$  depends on  $\alpha$ ,  $\beta$ ,  $M_{1450}^*$ , and  $C$ .
2. For a given  $\beta$  (e.g.  $\beta = -3.1$ ), the photon emissivity of quasars is a strong function of  $M_{1450}^*$ , but is not sensitive to  $\alpha$  as long as  $\alpha > -2.2$ . Note that  $\alpha$  is between  $-1.0$  and  $-2.0$  at low redshift.
3. In Equation 10,  $\dot{N}_{ion}(z)$  is a linear function of the clumping factor  $C$ , which is critical here to determine whether or not quasars alone can ionize the universe. If  $C = 30$  (Gnedin & Ostriker 1997), quasars can barely provide enough ionizing photons even if  $M_{1450}^* \geq -22$ . For a homogeneous

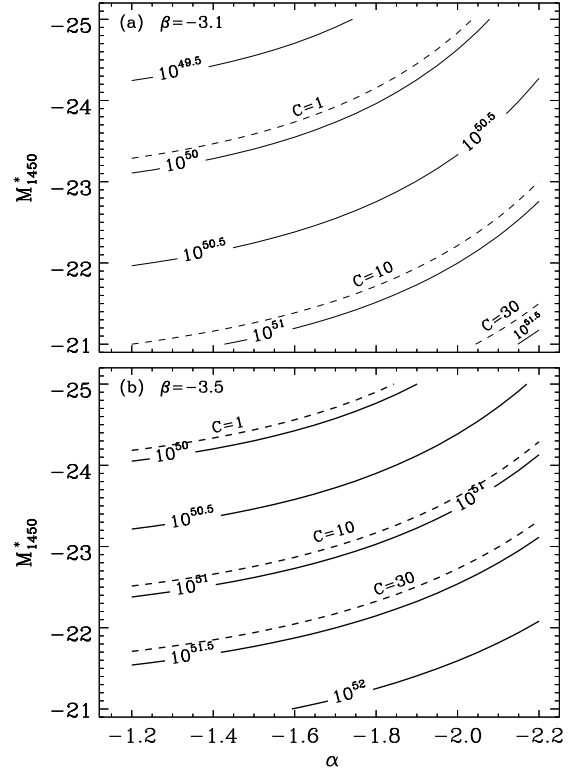


FIG. 7.— Photon emissivity (per unit comoving volume) from quasars as a function of the faint-end QLF slope  $\alpha$  and the characteristic luminosity  $M_{1450}^*$ . The solid lines represent the total photon emissivity from quasars. The dashed lines show the photon emissivity required to ionize the IGM at  $z \sim 6$  for the clumping factors  $C = 1$ ,  $C = 10$ , and  $C = 30$ , respectively. The upper panel is for the bright-end QLF slope  $\beta = -3.1$  and the lower panel is for  $\beta = -3.5$ .

IGM ( $C = 1$ ), however, quasars can easily provide enough ionizing photons.

4. The photon emissivity from quasars increases significantly as  $\beta$  steepens from  $-3.1$  to  $-3.5$ .

Since the total photon emissivity of quasars is not sensitive to  $\alpha$ , the quasar contribution to the reionization mainly depends on  $M_{1450}^*$  and  $C$  for a given  $\beta$ . It is clear that the quasar/AGN population can provide enough photons required to ionize the IGM only if the IGM is very homogeneous or the break luminosity is low. At low redshift,  $M_{1450}^*$  varies with redshift and the typical value is between  $-23$  and  $-21$ . At  $z \sim 6$ , the lower limit of  $M_{1450}^*$  is about  $-25$ . To measure  $M_{1450}^*$  at  $z \sim 6$ , much deeper surveys are needed. The clumping factor  $C$  is also poorly constrained. Previous studies used a range of values from 1 to  $\sim 100$ . If the typical value of  $C$  is 10–30 (e.g. Gnedin & Ostriker 1997; Madau et al. 1999), from Figure 7(a) the quasar population with  $\beta = -3.1$  is not likely to provide enough ionizing photons. However, if the reionization occurs outside-in and denser gas is ionized at a later time when most of the volume of the universe has been reionized, clumpiness does not significantly increase the number of photons required for reionization (Miralda-Escudé et al. 2000). In this case, the equivalent  $C$  is close to 1, and quasars can provide the required number of photons to ionize the IGM.

## 6. SUMMARY

We have discovered five quasars at  $z > 5.8$  in 260 deg<sup>2</sup> of the SDSS deep stripe, including one previously discovered by Venemans et al. (2007). The most distant one is at  $z = 6.12$ . These quasars were selected as *i*-dropout objects from the coadds of 10 SDSS imaging runs, going  $\sim 1.5$  magnitudes fainter than the SDSS main survey. The five quasars, with  $20 < z_{AB} < 21$ , are 1–2 magnitudes fainter than the luminous  $z \sim 6$  quasars found in the SDSS main survey. The Ly $\alpha$  emission lines in two quasars SDSS J0303–0019 and SDSS J2315–0023 are narrow (FWHM  $\sim 1600$  and  $2400$  km s<sup>-1</sup>) but strong (EW  $\sim 139$  and  $127$  Å), while the Ly $\alpha$  emission lines in another two quasars SDSS J0303–0019 and SDSS J2315–0023 are broad (FWHM  $\sim 7700$  and  $4900$  km s<sup>-1</sup>) but weak (EW  $\sim 36$  and  $17$  Å). The fifth one, SDSS J0353+0104, is a BAL quasar.

The new quasars, together with a previously discovered quasar, SDSS J0005–0006, comprise a flux-limited quasar sample with  $z_{AB} < 21$  at  $z \sim 6$  over 260 deg<sup>2</sup>. The sample covers the luminosity range  $-26.5 \leq M_{1450} \leq -25.4$ . The spatial density of the quasars at  $\langle z \rangle = 6.0$  and  $\langle M_{1450} \rangle = -25.8$  is  $(5.0 \pm 2.1) \times 10^{-9}$  Mpc<sup>-3</sup> mag<sup>-1</sup>. We use a single power-law form to model the bright-end QLF at  $z \sim 6$  and find a slope of  $-3.1 \pm 0.4$ , which is significantly steeper than the slope of the QLF at  $z \sim 4$ . Using the derived QLF, we find that the quasar/AGN population can provide enough photons required to ionize the IGM at  $z \sim 6$  only if the IGM is very homogeneous and the characteristic luminosity of the QLF is very low. To put better constraints on the quasar contribution, much deeper surveys are needed.

The quasars in this paper were selected from the SDSS coadded images with 5–18 runs. Currently the SDSS deep stripe has been scanned between 40 and 50 times, reaching 2  $\sim$  3 magnitudes deeper than the main survey when co-added. We are performing a deeper survey of

$z \sim 6$  quasars down to  $z_{AB} \sim 22$  in this region. We expect to obtain a flux-limited sample with  $z_{AB} < 22$  in the next few years.

We acknowledge support from NSF grant AST-0307384, a Sloan Research Fellowship and a Packard Fellowship for Science and Engineering (LJ, XF). We thank the MMT staff, Magellan staff, and Keck staff for their expert help in preparing and carrying out the observations.

Funding for the SDSS and SDSS-II has been provided by the Alfred P. Sloan Foundation, the Participating Institutions, the National Science Foundation, the U.S. Department of Energy, the National Aeronautics and Space Administration, the Japanese Monbukagakusho, the Max Planck Society, and the Higher Education Funding Council for England. The SDSS Web Site is <http://www.sdss.org/>. The SDSS is managed by the Astrophysical Research Consortium for the Participating Institutions. The Participating Institutions are the American Museum of Natural History, Astrophysical Institute Potsdam, University of Basel, Cambridge University, Case Western Reserve University, University of Chicago, Drexel University, Fermilab, the Institute for Advanced Study, the Japan Participation Group, Johns Hopkins University, the Joint Institute for Nuclear Astrophysics, the Kavli Institute for Particle Astrophysics and Cosmology, the Korean Scientist Group, the Chinese Academy of Sciences (LAMOST), Los Alamos National Laboratory, the Max-Planck-Institute for Astronomy (MPIA), the Max-Planck-Institute for Astrophysics (MPA), New Mexico State University, Ohio State University, University of Pittsburgh, University of Portsmouth, Princeton University, the United States Naval Observatory, and the University of Washington.

## REFERENCES

- Adelman-McCarthy, J. K., et al. 2007a, ApJS, in press (astro-ph/0707.3380)  
 Adelman-McCarthy, J. K., et al. 2007b, ApJS, submitted (astro-ph/0707.3413)  
 Avni, Y., & Bahcall, J. N. 1980, ApJ, 235, 694  
 Barth, A. J., Martini, P., Nelson, C. H., & Ho, L. C. 2003, ApJ, 594, L95  
 Becker, R. H., White, R. L., & Helfand, D. J. 1995, ApJ, 450, 559  
 Becker, R. H., et al. 2001, AJ, 122, 2850  
 Bertin, E., Mellier, Y., Radovich, M., Missonnier, G., Didelon, P., & Morin, B. 2002, Astronomical Data Analysis Software and Systems XI, 281, 228  
 Bouwens, R. J., Illingworth, G. D., Blakeslee, J. P., & Franx, M. 2006, ApJ, 653, 53  
 Boyle, B. J., Shanks, T., Croom, S. M., Smith, R. J., Miller, L., Loaring, N., & Heymans, C. 2000, MNRAS, 317, 1014  
 Bunker, A. J., Stanway, E. R., Ellis, R. S., & McMahon, R. G. 2004, MNRAS, 355, 374  
 Chiu, K., Fan, X., Leggett, S. K., Golimowski, D. A., Zheng, W., Geballe, T. R., Schneider, D. P., & Brinkmann, J. 2006, AJ, 131, 2722  
 Cool, R. J., et al. 2006, AJ, 132, 823  
 Dijkstra, M., Haiman, Z., & Loeb, A. 2004, ApJ, 613, 646  
 Djorgovski, S. G., Castro, S., Stern, D., & Mahabal, A. A. 2001, ApJ, 560, L5  
 Douglas, L. S., Bremer, M. N., Stanway, E. R., & Lehnert, M. D. 2007, MNRAS, 376, 1393  
 Elston, R. J., et al. 2006, ApJ, 639, 816  
 Fan, X. 1999, AJ, 117, 2528  
 Fan, X., et al. 2000, AJ, 120, 1167  
 Fan, X., et al. 2001a, AJ, 122, 2833  
 Fan, X., et al. 2001b, AJ, 121, 31  
 Fan, X., Narayanan, V. K., Strauss, M. A., White, R. L., Becker, R. H., Pentericci, L., & Rix, H.-W. 2002, AJ, 123, 1247  
 Fan, X., et al. 2003, AJ, 125, 1649  
 Fan, X., et al. 2004, AJ, 128, 515  
 Fan, X., et al. 2006a, AJ, 131, 1203  
 Fan, X., et al. 2006b, AJ, 132, 117  
 Fan, X., Carilli, C. L., & Keating, B. 2006c, ARA&A, 44, 415  
 Fontanot, F., et al. 2007, A&A, 461, 39  
 Fukugita, M., Ichikawa, T., Gunn, J. E., Doi, M., Shimasaku, K., & Schneider, D. P. 1996, AJ, 111, 1748  
 Gnedin, N. Y., & Ostriker, J. P. 1997, ApJ, 486, 581  
 Golimowski, D. A., et al. 2004, AJ, 127, 3516  
 Goto, T. 2006, MNRAS, 371, 769  
 Gunn, J. E., & Peterson, B. A. 1965, ApJ, 142, 1633  
 Gunn, J. E., et al. 1998, AJ, 116, 3040  
 Gunn, J. E., et al. 2006, AJ, 131, 2332  
 Hogg, D. W., Finkbeiner, D. P., Schlegel, D. J., & Gunn, J. E. 2001, AJ, 122, 2129  
 Hopkins, P. F., Hernquist, L., Cox, T. J., Di Matteo, T., Martini, P., Robertson, B., & Springel, V. 2005, ApJ, 630, 705  
 Hopkins, P. F., Richards, G. T., & Hernquist, L. 2007, ApJ, 654, 731  
 Ivezić, Ž., et al. 2004, AN, 325, 583  
 Jannuzi, B. T., & Dey, A. 1999, in ASP Conf. Ser. 191, Photometric Redshifts and High-Redshift Galaxies, ed. R. J. Weymann, L. J. Storrie-Lombardi, M. Sawicki, & R. J. Brunner (San Francisco: ASP), 111  
 Jiang, L., et al. 2006a, AJ, 132, 2127  
 Jiang, L., et al. 2006b, AJ, 131, 2788  
 Jiang, L., et al. 2007, AJ, 134, 1150  
 Kashikawa, N., et al. 2006, ApJ, 648, 7  
 Knapp, G. R., et al. 2004, AJ, 127, 3553  
 Kurk, J. D. et al. 2007, ApJ, in press (astro-ph/0707.1662)  
 Li, Y., et al. 2007, ApJ, 665, 187  
 Lupton, R. H., Gunn, J. E., & Szalay, A. S. 1999, AJ, 118, 1406

- Lupton, R. H., Gunn, J. E., Ivezić, Ž., Knapp, G. R., Kent, S., & Yasuda, N. 2001, in *Astronomical Data Analysis Software and Systems X*, edited by F. R. Harnden Jr., F. A. Primini, and H. E. Payne, ASP Conference Proceedings, 238, 269
- Madau, P., Haardt, F., & Rees, M. J. 1999, *ApJ*, 514, 648
- Mahabal, A., Stern, D., Bogosavljević, M., Djorgovski, S. G., & Thompson, D. 2005, *ApJ*, 634, L9
- Maiolino, R., Juarez, Y., Mujica, R., Nagar, N. M., & Oliva, E. 2003, *ApJ*, 596, L155
- McGreer, I. D., Becker, R. H., Helfand, D. J., & White, R. L. 2006, *ApJ*, 652, 157
- McQuinn, M., Hernquist, L., Zaldarriaga, M., & Dutta, S. 2007, *MNRAS*, in press (astro-ph/0704.2239)
- Meiksin, A. 2005, *MNRAS*, 356, 596
- Miralda-Escudé, J., Haehnelt, M., & Rees, M. J. 2000, *ApJ*, 530, 1
- Oke, J. B., & Gunn, J. E. 1983, *ApJ*, 266, 713
- Page, M. J., & Carrera, F. J. 2000, *MNRAS*, 311, 433
- Pier, J. R., Munn, J. A., Hindsley, R. B., Hennessy, G. S., Kent, S. M., Lupton, R. H., & Ivezić, Ž. 2003, *AJ*, 125, 1559
- Richards, G. T., et al. 2004, *AJ*, 127, 1305
- Richards, G. T., et al. 2005, *MNRAS*, 360, 839
- Richards, G. T., et al. 2006, *AJ*, 131, 2766
- Salvaterra, R., Haardt, F., & Volonteri, M. 2007, *MNRAS*, 374, 761
- Schneider, D. P., Schmidt, M., & Gunn, J. E. 1991, *AJ*, 101, 2004
- Shankar, F., & Mathur, S. 2007, *ApJ*, 660, 1051
- Sheinis, A. I., Bolte, M., Epps, H. W., Kibrick, R. I., Miller, J. S., Radovan, M. V., Bigelow, B. C., & Sutin, B. M. 2002, *PASP*, 114, 851
- Shen, Y., et al. 2007, *AJ*, 133, 2222
- Skrutskie, M. F., et al. 2006, *AJ*, 131, 1163
- Smith, J. A., et al. 2002, *AJ*, 123, 2121
- Spiegel, D. N., et al. 2007, *ApJS*, 170, 377
- Srbínovsky, J. A., & Wyithe, J. S. B. 2007, *MNRAS*, 374, 627
- Stoughton, C., et al. 2002, *AJ*, 123, 485
- Trump, J. R., et al. 2006, *ApJS*, 165, 1
- Tucker, D., et al. 2006, *AN*, 327, 821
- Vanden Berk, D. E., et al. 2001, *AJ*, 122, 549
- Venemans, B. P., McMahon, R. G., Warren, S. J., Gonzalez-Solares, E. A., Hewett, P. C., Mortlock, D. J., Dye, S., & Sharp, R. G. 2007, *MNRAS*, 376, L76
- Vestergaard, M. 2004, *ApJ*, 601, 676
- Volonteri, M., & Rees, M. J. 2006, *ApJ*, 650, 669
- Warren, S. J., et al. 2007, *MNRAS*, 375, 213
- Willott, C. J., Delfosse, X., Forveille, T., Delorme, P., & Gwyn, S. D. J. 2005, *ApJ*, 633, 630
- Willott, C. J., *AJ*, submitted (astro-ph/0706.0914)
- Wyithe, J. S. B., & Loeb, A. 2003, *ApJ*, 595, 614
- Wyithe, J. S. B., & Padmanabhan, T. 2006, *MNRAS*, 372, 1681
- Yan, H., & Windhorst, R. A. 2004, *ApJ*, 612, L93
- York, D. G., et al. 2000, *AJ*, 120, 1579
- Zheng, W., Kriss, G. A., Telfer, R. C., Grimes, J. P., & Davidsen, A. F. 1997, *ApJ*, 475, 469